polysaccharides

MDPI

Article

Size-Dependent Diffusive Transport in Alkali-Insolubilized Konjac Glucomannan Free-Standing Membranes

Misaki Morota [1], Keita Kashima [2] and Masahide Hagiri [1,*]

[1] Department of Chemistry and Materials Science, Gunma College, National Institute of Technology, 580 Toribamachi, Maebashi 371-8530, Gunma, Japan
[2] Department of Materials Chemistry and Bioengineering, Oyama College, National Institute of Technology, 771 Nakakuki, Oyama 323-0806, Tochigi, Japan
* Correspondence: hagiri@gunma-ct.ac.jp

Abstract

As the demand for sustainable and bio-based alternatives to petroleum-derived membranes grows, polysaccharides have emerged as promising candidates. In this study, we fabricated free-standing membranes from konjac glucomannan (KGM), a neutral polysaccharide, using a simple base-induced insolubilization process. Fourier transform infrared spectroscopy revealed that the deacetylation of KGM chains promotes extensive intermolecular hydrogen bonding, creating a robust and stable three-dimensional network without the need for chemical cross-linkers. The resulting KGM free-standing membranes exhibited excellent mechanical properties, characterized by high tensile strength in the dry state and remarkable flexibility when hydrated. Furthermore, the membranes demonstrated superior chemical resistance to organic solvents such as acetone and n-hexane. Transport studies showed that the membranes possess a highly dense structure with no detectable pressure-driven pure-water permeation up to 0.25 MPa. Solute permeation experiments using eight model molecules (molecular weight = 144–14,600 Da) indicated that transport behavior is consistent with diffusion through a hydrated polymer network. The effective diffusion coefficient D_{eff} showed a strong correlation with molecular weight M, following the relationship $D_{eff} \propto M^{-1.7}$. Furthermore, the permeation behavior remained stable across a wide pH range (2–12), and, within the investigated range of monovalent solutes, D_{eff} was insensitive to solute charge, indicating that mass transport is dominated by size-based diffusion rather than electrostatic interactions. These findings suggest that KGM free-standing membranes enable reliable molecular fractionation based on size-dependent diffusion within a stable, neutral matrix, offering significant potential for sustainable separation technologies and biomedical applications.

Keywords: Konjac Glucomannan; polysaccharide-based membrane; size-dependent molecular diffusion; diffusion-selective transport

Check for updates

Academic Editor: Tina Maver

Received: 9 February 2026
Revised: 17 March 2026
Accepted: 3 April 2026
Published: 6 April 2026

Copyright: © 2026 by the authors. Licensee MDPI, Basel, Switzerland. This article is an open access article distributed under the terms and conditions of the Creative Commons Attribution (CC BY) license.

1. Introduction

Since the late 1960s, membrane separation has been widely adopted for purification and fractionation because it enables separations with lower energy consumption and milder operating conditions than conventional thermal processes such as distillation and evaporation. As demands for energy efficiency and environmental sustainability continue to increase, growing attention has been directed toward replacing petroleum-derived membrane materials with renewable, bio-based alternatives [1].

Synthetic polymers provide excellent mechanical strength, durability, and processability; however, their large-scale production and disposal have contributed to persistent plastic pollution in terrestrial and marine environments. These concerns have intensified efforts to develop sustainable membrane materials derived from renewable biomass resources [2–5]. Among various candidates, polysaccharides are particularly attractive owing to their abundance, biodegradability, and generally favorable biocompatibility [6,7]. Consequently, polysaccharide-based membranes have been actively explored for applications including packaging, biomedical devices, and water-treatment technologies [3,8–10].

To date, research on polysaccharide membranes has largely focused on cellulose, chitosan, and alginate. Cellulose, the most abundant polysaccharide on Earth, is highly crystalline and mechanically robust, which underpins its widespread use in dialysis and ultrafiltration membranes as well as packaging films [11–13]. Chitosan, derived from deacetylation of chitin, possesses amino groups giving rise to cationic character, pH responsiveness, and antibacterial activity. These unique characteristics make it an excellent candidate for various applications, including adsorbents, separation materials, and biomedical devices [2,14,15]. Alginate membranes cross-linked with calcium ions have also been reported to exhibit sharp molecular fractionation in the low-molecular-weight region, and their porous structure and pure-water permeability can be further tuned by incorporating oligoethylene glycol or polyethylene glycol [16–18]. Despite these advances, comparatively few studies have explored membrane separation materials derived from polysaccharides other than cellulose, chitosan, and alginate, indicating opportunities to broaden the range of sustainable membrane materials.

In this context, we focus on konjac glucomannan (KGM), a water-soluble, electrically neutral polysaccharide obtained mainly from the konjac plant (*Amorphophallus konjac*). KGM is composed primarily of β-D-mannose and β-D-glucose units and possesses a characteristic molecular architecture, featuring occasional β-1,3-linked branching structures accounting for approximately 8% of the backbone, as well as acetyl substituents occurring at a frequency of one per 9–19 sugar residues [19–21]. KGM is widely used in the food industry as a thickener and emulsifier. Notably, alkaline deacetylation of KGM enhances intermolecular hydrogen bonding and induces thermally irreversible gelation [21], suggesting a promising route to fabricate water-insoluble and mechanically stable membranes without chemical cross-linkers.

KGM has also attracted attention in biomedical and packaging-related applications, including drug delivery systems, tissue engineering scaffolds, and functional films incorporating antimicrobial or barrier-enhancing additives [21–26]. Huang et al. demonstrated that hybrid hydrogels composed of Fmoc-diphenylalanine (Fmoc-FF) and KGM exhibit high stability and mechanical robustness, enabling sustained and controlled release of hydrophobic drugs [21]. Thangavel et al. developed a biocompatible scaffold based on KGM and silk fibroin (SF), which promotes neovascularization [23]. Wu et al. showed that incorporation of chitosan/gallic acid nanoparticles into KGM films imparted excellent antimicrobial activity [24]. In addition, Zhang et al. reported that the addition of SiO_2 to KGM/carrageenan films significantly enhanced their mechanical strength as well as their water vapor and gas barrier properties [25,26]. However, despite these functional studies, systematic investigations of solute transport and separation behavior in KGM-based membranes remain limited.

In the present study, we prepare free-standing KGM membranes via alkaline insolubilization and systematically evaluate their structural, mechanical, and transport properties relevant to membrane separation. Mechanical properties under dry and wet conditions, water vapor permeability, and resistance to organic solvents were examined. Transport performance is analyzed using two complementary approaches: pressure-driven pure-

water permeation to assess hydraulic permeability, and concentration-gradient-driven solute permeation to quantify molecular-weight-dependent diffusion behavior. By correlating permeability behavior with molecular weight, this work elucidates size-dependent mass transport in hydrated KGM membranes and highlights their potential as bio-based separation materials with a neutral and chemically stable matrix.

2. Materials and Methods

2.1. Materials

Potassium hydroxide (special grade, KANTO CHEMICAL Co., Inc., Tokyo, Japan), sodium hydroxide (special grade, FUJIFILM Wako Pure Chemical Corp., Osaka, Japan), 8 mol L^{-1} potassium hydroxide aqueous solution (FUJIFILM Wako Pure Chemical Corp., Osaka, Japan), 8 mol L^{-1} sodium hydroxide aqueous solution (FUJIFILM Wako Pure Chemical Corp., Osaka, Japan), anhydrous calcium chloride (KANTO CHEMICAL Co., Inc., Tokyo, Japan), sulfuric acid (KANTO CHEMICAL Co., Inc., Tokyo, Japan), phenol (special grade, FUJIFILM Wako Pure Chemical Corp., Osaka, Japan), phosphoric acid (special grade, FUJIFILM Wako Pure Chemical Corp., Osaka, Japan), boric acid (special grade, KANTO CHEMICAL Co., Inc., Tokyo, Japan), 1 mol L^{-1} acetic acid aqueous solution (FUJIFILM Wako Pure Chemical Corp., Osaka, Japan) were used as received. Sodium benzoate (KANTO CHEMICAL Co., Inc., Tokyo, Japan), Methyl Orange (Koso Kagakuyaku Holdings Co., Ltd., Tokyo, Japan), Neutral Red (FUJIFILM Wako Pure Chemical Corp., Osaka, Japan), Bordeaux S (FUJIFILM Wako Pure Chemical Corp., Osaka, Japan), Brilliant Blue FCF (FUJIFILM Wako Pure Chemical Corp., Osaka, Japan), Rose Bengal (Sigma-Aldrich Co. LLC, St. Louis, MO, USA), Sirius Red (FUJIFILM Wako Pure Chemical Corp., Osaka, Japan), Dextran T3 (MedChemExpress LLC, Monmouth Junction, NJ, USA), lysozyme (from egg white; NACALAI TESQUE, Inc., Kyoto, Japan), and a TaKaRa Bradford Protein Assay Kit (Takara Bio Inc., Shiga, Japan) were used as model solutes or reagents for permeation and concentration analyses. Konjac glucomannan (KGM) was obtained as a commercial product (PROPOL-A, Shimizu Chemical Corp., Hiroshima, Japan), derived from *Amorphophallus konjac*, and was used without further purification.

2.2. Preparation of KGM Free-Standing Membranes

A 1.0 wt% aqueous solution of KGM derived from *Amorphophallus konjac* was prepared. The solution was agitated and deaerated using a rotary mixer (AR-100, THINKY Corp., Tokyo, Japan) for 4 min to ensure homogeneity and removal of entrapped air, and subsequently cast onto a glass Petri dish. The mass of KGM solution applied per unit area was 4.3×10^3 g m^{-2}. The cast films were dried for at least 24 h at 25.0 °C and 50% relative humidity in a small environmental test chamber (SH-222, ESPEC Corp., Osaka, Japan). Insolubilization of the dried KGM films was achieved by alkaline treatment to promote deacetylation. The films were immersed in a 2.5 M potassium hydroxide aqueous solution for 4 min and then thoroughly washed with deionized water. To stabilize the membrane structure, the films were further immersed in deionized water at 70 °C for 4 min, followed by repeated washing with deionized water. After these treatments, the films became water-insoluble and could be handled as self-supporting, free-standing membranes, hereafter referred to as KGM free-standing membranes.

The preparation conditions were optimized by systematically varying the potassium hydroxide concentration and treatment duration. The thickness and water content of the resulting KGM free-standing membranes were found to be largely independent of potassium hydroxide concentrations between 2.5 and 4 M and treatment times of 4 min or longer, indicating that deacetylation sufficient for membrane insolubilization proceeds rapidly under these conditions. Detailed optimization results are provided in the Supporting Information.

2.3. Characterization of KGM Free-Standing Membranes

The cross-sectional morphology of the KGM free-standing membranes prepared as described in Section 2.2 was characterized by scanning electron microscopy (SEM, JCM7000, JEOL Ltd., Tokyo, Japan). Membrane samples were cut in the dry state to expose fresh cross sections prior to observation.

To assess structural modifications of the glycan framework induced by the insolubilization process, ATR-FTIR spectra were acquired before and after alkaline treatment using an attenuated total reflectance Fourier transform infrared (ATR–FT-IR) spectrophotometer (FT-IR6800, JASCO Corp., Tokyo, Japan) equipped with an attenuated total reflectance (ATR) accessory. Non-insolubilized reference films were prepared by casting a 1.0 wt% aqueous KGM solution into a container and drying it for at least 24 h. Insolubilized membrane samples were prepared according to the procedure described in Section 2.2 and analyzed in the dried state without further chemical treatment.

2.4. Mechanical Properties Test

The tensile strength and tensile strain of the KGM free-standing membranes prepared as described in Section 2.2 were evaluated under dry and wet conditions. Dry-state measurements were performed on membranes equilibrated under ambient laboratory conditions. For the dry-state measurements, membrane specimens were cut into No. 3 dumbbell-shaped specimens [27]. The thickness of each specimen was measured at five positions within the gauge length (20 mm) using a dial thickness gauge (547-401A, Mitutoyo Corp., Kanagawa, Japan), and the average thickness was calculated. The upper and lower 15 mm sections outside the gauge length of each specimen were fixed using a mechanical jig, and tensile tests were performed using a bench-top tensile and compression testing machine (MCT-1150, A&D Co., Ltd., Tokyo, Japan) at a crosshead speed of 10 mm min^{-1}. For the wet-state measurements, membrane samples were immersed in deionized water overnight ($\geq$12 h) at room temperature. The hydrated samples were then cut into No. 3 dumbbell-shaped specimens, and excess surface water was removed by gently blotting both sides once with lint-free paper (Kimwipe, Nippon Paper Crecia Co., Ltd., Tokyo, Japan). The specimen thickness was measured at five positions within the 20 mm gauge length in the same manner as for the dry samples. Tensile tests were conducted at room temperature (25 °C) under air-conditioned laboratory conditions, using the same testing parameters as those employed for the dry-state measurements.

The tensile strength σ [MPa] was calculated using Equation (1), where F [N] is the force at break and A [mm^2] is the cross-sectional area of the specimen determined from the average film thickness:

$$\sigma = \frac{F}{A} \quad (1)$$

The tensile strain ε [%] was calculated using Equation (2), where L_0 [mm] is the initial gauge length between the marked lines and ΔL [mm] is the elongation at break [28]:

$$\varepsilon = \frac{\Delta L}{L_0} \cdot 100 \quad (2)$$

For each condition, ten independent specimens (n = 10) were tested, and the mean values and standard deviations were calculated. For comparison, identical tensile tests were performed on polyvinylidene chloride film (PVDC, Asahi Kasei Corp., Tokyo, Japan) and regenerated cellulose film (RC, Visking tubing; Nihon Medical Science Co., Ltd., Tokyo, Japan).

2.5. Determination of Water Vapor Permeability (WVP)

The water vapor permeability (WVP) of KGM free-standing membranes was evaluated. The membranes were prepared and thoroughly dried as described in Section 2.2, and WVP measurements were conducted in accordance with the Japanese Industrial Standard JIS Z 0208 [29].

Each KGM free-standing membrane was cut into a circular specimen with a diameter of 60 mm. The film thickness was measured at five positions using a dial thickness gauge (547-401A, Mitutoyo Corp., Kanagawa, Japan), and the mean thickness l [m] and standard deviation were calculated. WVP measurements were performed using a moisture permeability cup (Elcometer 5100, Elcometer Ltd., Manchester, UK) with an effective permeation area $A = 1.0 \times 10^{-3}$ m^2. The cup was filled with 2.0 g of anhydrous calcium chloride as a desiccant to maintain 0% relative humidity inside the cup. A cut membrane specimen was placed over the opening of the cup, which was then sealed with a packing. After recording the initial mass of the assembled cup, it was placed in a small environmental test chamber (SH-222, ESPEC Corp., Osaka, Japan) maintained at 40.0 °C and 90% relative humidity. The mass of the cup was recorded at predetermined time intervals. The initial mass of the cup was defined as w_0 [kg], and the mass increase Δw [kg] was plotted as a function of elapsed time t [s]. The rate of mass change Δm [kg s^{-1}] was obtained from the slope of the linear region of the Δw [kg] versus t plot. Linear fitting was performed using data collected while the calcium chloride remained in the solid state, prior to deliquescence due to moisture absorption. The WVP [kg m^{-1} s^{-1} Pa^{-1}] was calculated using Equation (3):

$$\mathrm{WVP}\left[\mathrm{kg\,m^{-1}s^{-1}Pa^{-1}}\right] = \frac{\Delta m\, l}{A\,\Delta p} \tag{3}$$

where Δp [Pa] is the difference in the partial pressure of water vapor between inside and outside of the cup, as determined by the temperature and relative humidity conditions [30,31].

Measurements were performed using three independent KGM free-standing membrane specimens (n = 3), and the mean values and standard deviations were calculated [29]. For comparison, identical WVP measurements were conducted for PVDC film and RC film.

2.6. Resistance to Organic Solvents

The KGM free-standing membranes prepared as described in Section 2.2 were cut into square specimens with dimensions of 18 mm × 18 mm. A total of six independent specimens were prepared and their initial masses w_0 [g] were measured. The film thickness l_0 [mm] of each specimen was measured at three positions using a dial thickness gauge (547-401A, Mitutoyo Corp., Kanagawa, Japan), and the average thickness was calculated. Each specimen was placed individually into a 25 mL glass tube containing 10 mL of either acetone or *n*-hexane, and the tubes were sealed. For each solvent, three tubes corresponding to immersion times of 30 min, 60 min, and 24 h were prepared. After each immersion period, the specimens were removed from the solvent, excess surface liquid was gently wiped off using lint-free paper. The mass w [g] and thickness l [mm] were measured again at the same positions. For each immersion time, the mean values and standard deviations of w and l were calculated. Changes in mass and thickness relative to the initial values (w_0 and l_0) were used to evaluate solvent-induced swelling, dissolution, or dimensional instability, thereby assessing the resistance of the KGM membranes to organic solvents.

2.7. Evaluation of Pure Water Permeability and Estimation of Effective Size of Water Permeation Channels

The pure water permeability of KGM free-standing membranes prepared as described in Section 2.2 was evaluated by a constant-pressure filtration method, following the proce-

dure reported by our group [32]. The membranes were cut into circular specimens with a diameter of 25 mm and mounted in a polypropylene membrane filter holder (SWINNEX25, Merck Millipore Corp., Burlington, MA, USA) with an effective permeation area $A = 4.15 \times 10^{-4}$ m^2. The filter holder was connected to a laboratory-scale pressure vessel (baby tank; BT-600P, ADVANTEC Co., Ltd., Tokyo, Japan) made of pressure-resistant polyethersulfone. The vessel was filled with pure water and pressurized using nitrogen gas to apply a uniform pressure to the membrane. The operating pressure Δp [MPa] was varied in the range of 0.050–0.25 MPa. The permeated mass w_p [kg] was monitored using an electronic balance (UW4200H, Shimadzu Corp., Kyoto, Japan) as a function of time.

Under all applied pressure conditions, no visible permeation of pure water was observed, and no droplet formation was detected at the permeate outlet throughout the measurement period. Based on this observation, the permeated water volume was considered to be smaller than the volume corresponding to a single water droplet, and the permeation rate was therefore below the practical detection limit of the present experimental setup. Accordingly, the maximum permeated mass was conservatively estimated as being less than the mass of a single water droplet during the measurement time window, and this value was used to define an upper bound for pressure-driven water transport.

The effective size of water permeation channel (hydraulic pore radius) r [m] of the membrane was calculated using the Guéout-Bjerrum-Manegold equation as shown in Equation (4):

$$r = \sqrt{\frac{24\eta L K_F}{\varepsilon}} \tag{4}$$

where η [Pa s] is the viscosity of the permeate, L [m] is the film thickness, K_F [m^3 N^{-1} s^{-1}] is the filtration coefficient estimated from the upper limit of permeation defined by the absence of droplet formation, and ε [-] is the volumetric void fraction of the membrane [12,33,34]. In this study, the calculated hydraulic channel radius represents an upper bound rather than an exact value, reflecting the absence of detectable pressure-driven water permeation under the investigated conditions.

2.8. Effective Diffusion Coefficient of Molecules in the Membrane

To evaluate the permeability of the prepared membranes, the effective diffusion coefficient in the membrane, D_{eff}, was determined using a membrane permeation method based on a concentration-gradient-driven diffusion experiment, following the procedure reported by Kashima et al. [16].

KGM membranes prepared as described in Section 2.2 were mounted in glass mass transfer cells and immersed in a glass water bath maintained at 25 °C using an immersion-type thermostatic device (BF200, Yamato Scientific Co., Ltd., Tokyo, Japan). For each experiment, 250 mL of an aqueous solution of a model molecule was added to the feed side of the cell, while 250 mL of pure water was added to the permeate side. Both sides of the cell were agitated using stirring motors (BL1200, SHINTO Scientific Co., Ltd., Tokyo, Japan) equipped with six-blade turbine impellers with a diameter of 3 cm, operated at a rotation speed of 900 rpm. These conditions were employed to minimize external mass-transfer resistance at the membrane interfaces. After a predetermined permeation time, a 2.0 mL aliquot of solution was collected from each compartment for concentration analysis. Sodium benzoate (144.1 Da), Methyl Orange (327.4 Da), Bordeaux S (604.5 Da), Brilliant Blue FCF (792.9 Da), Rose Bengal (1018 Da), Sirius Red (1373 Da), Dextran T3 (3000 Da), and lysozyme (14,600 Da) were used as model solutes spanning a wide range of molecular weights. The initial concentrations of the model molecule solutions were set to 1.0 mM for sodium benzoate, Methyl Orange, Bordeaux S, Brilliant Blue FCF, Rose Bengal, and lysozyme; 10 mM for Sirius Red; and 5.0 mM for Dextran T3.

The concentrations of the feed-side solutions at $t = 0$ s and the permeate-side solutions at each sampling time were determined by UV–visible absorbance measurements. The absorbance of sodium benzoate was measured using a UV-visible spectrophotometer (V-560, JASCO Corp., Tokyo, Japan) at a wavelength of 253 nm, and the concentration was calculated using a calibration curve prepared in advance. The absorbance of Methyl Orange was measured at 450 nm, Bordeaux S, Rose Bengal, and Sirius Red at 540 nm, and Brilliant Blue FCF at 630 nm using a microplate reader (MPR-A100T, AS ONE Corp., Osaka, Japan). All absorbance measurements were performed in triplicate wells, and averaged values were used for concentration determination. The concentration of Dextran T3 was determined using the phenol–sulfuric acid method. Briefly, 100 µL of a 5 wt% phenol solution was added to 40 µL of the sample solution and allowed to stand for 10 min at room temperature. Subsequently, 200 µL of concentrated sulfuric acid was added, and the mixture was left to react for 15 min. The absorbance was then measured at 490 nm using a microplate reader (SH-1300Lab, CORONA ELECTRIC Corp., Ibaraki, Japan). A dilution series of Dextran T3 was prepared in parallel, and concentrations were determined from the calibration curve. Absorbance measurements were performed in triplicate wells, and the averaged values were used for concentration determination. The concentration of lysozyme was determined using the Bradford method. In this assay, 100 µL of TaKaRa Bradford Protein Assay Kit (Takara Bio Inc., Shiga, Japan) was added to 100 µL of the lysozyme solution and allowed to react at 25 °C for 5 min. A dilution series of lysozyme standard solutions was prepared simultaneously, and the absorbance of both the permeate samples and standards was measured at 595 nm using a microplate reader (SH-1300Lab, CORONA ELECTRIC Corp., Ibaraki, Japan). Concentrations were determined from the corresponding calibration curve. Absorbance measurements were performed in triplicate wells, and the averaged values were used for concentration determination.

A schematic diagram of the membrane permeation test apparatus is shown in Figure 1.

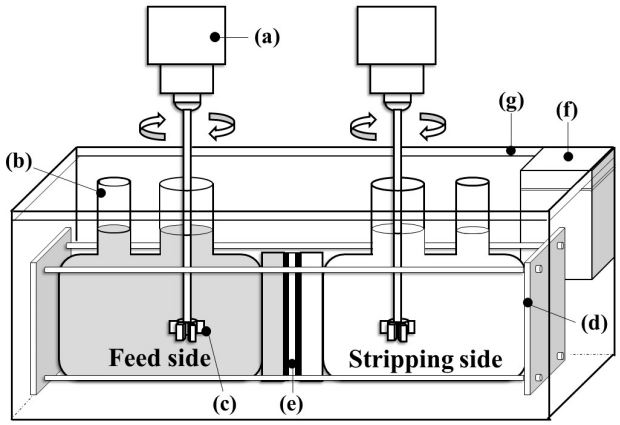


Figure 1. Schematic of membrane mass-transfer apparatus. (a) Stirring motor. (b) Glass mass-transfer cells, between which the membrane was mounted. (c) Six-blade turbine impeller (diameter: 3 cm). (d) Cell Holder. (e) Konjac glucomannan (KGM) free-standing membrane (diameter: 5.5 cm). (f) Immersion-type thermostatic device, maintaining the water temperature at 25 °C. (g) Glass water bath.

The mass transfer through the membrane driven by a concentration gradient can be described by the model schematic shown in Figure 2. When the molar transfer rate from the feed side to the permeate side is defined as N [mol s^{-1}], the mass balance equations for the feed-side boundary layer, the membrane interior, and the permeate-side boundary layer can be expressed by Equation (5), Equation (6), and Equation (7), respectively:

$$N = A\, k_{L1}\, (C_F - C_{M1}) \quad (5)$$

$$N = A\, k_M\, (C_{M1} - C_{M2}) \tag{6}$$

$$N = A\, k_{L2}\, (C_{M2} - C_S) \tag{7}$$

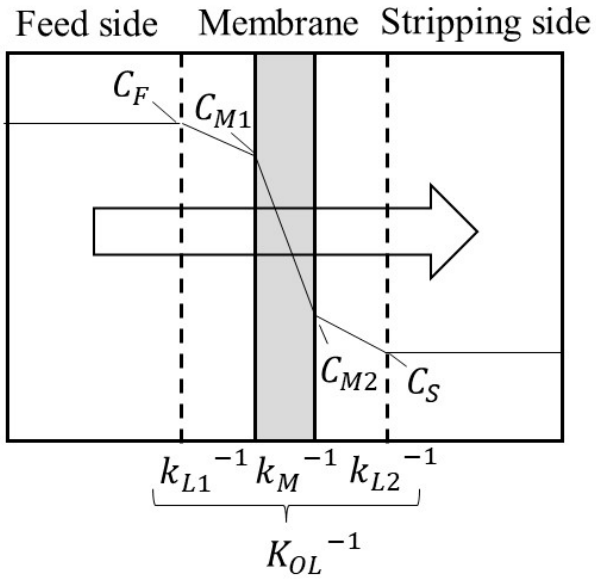


Figure 2. Schematic diagram of mass transport near and across the membrane.

Here, A [m^2] is the effective area for mass transfer, k_{L1} [m s^{-1}] is the mass transfer coefficient at the feed-side boundary layer, k_M [m s^{-1}] is the mass transfer coefficient within the membrane, and k_{L2} [m s^{-1}] is the mass transfer coefficient at the permeate-side boundary layer. C_F [M] is the solute concentration in the bulk feed solution, C_{M1} [M] is the solute concentration at the membrane surface on the feed side, C_{M2} [M] is the solute concentration at the membrane surface on the permeate side, and C_S [M] is the solute concentration in the bulk permeate solution.

The overall mass transfer coefficient, K_{OL} [m s^{-1}], is defined as the reciprocal of the sum of the resistances associated with the feed-side boundary layer, the membrane interior, and the permeate-side boundary layer. Under the assumption that the decrease in solute concentration on the feed side equals the increase on the permeate side, the molar transfer rate N can be expressed using the initial feed-side concentration C_{fi} [M], as shown in Equation (8):

$$N = A\, K_{OL} \left(C_{fi} - 2C_S\right) \tag{8}$$

Assuming that the permeate volume V [m^3] remains constant, the temporal change in the permeate-side concentration C_S can be expressed as Equation (9):

$$\frac{dC_S}{dt} = \frac{A}{V} K_{OL} \left(C_{fi} - 2C_S\right) \tag{9}$$

Integration of Equation (9) from $t = 0$ to t yields Equation (10):

$$\int_0^{C_S} \frac{dC_S}{\left(C_{fi} - 2C_S\right)} = \int_0^t \frac{A}{V} K_{OL}\, dt = \frac{A}{V} K_{OL}\, t$$

$$\ln\left(1 - \frac{2C_S}{C_{fi}}\right) = -\frac{2\, A\, K_{OL}}{V} t \tag{10}$$

The overall mass transfer coefficient K_{OL} was obtained from the slope of the linear relationship between elapsed time t [s] and the left-hand side of Equation (10). Under sufficiently turbulent conditions, external mass transfer resistances become negligible, and

K_{OL} can be approximated as the mass transfer coefficient within the membrane, k_M. Accordingly, the effective diffusion coefficient in the membrane, D_{eff} [m^2 s^{-1}], was calculated from the membrane thickness l [m] using Equation (11):

$$k_M = \frac{D_{eff}}{l} \tag{11}$$

Stirring conditions were selected in accordance with the protocol reported by Kashima et al. [16], and the dimensions, thickness, and materials of the permeation cells were identical to those used in their previous study.

As a reference, the diffusion coefficient of each solute in water, D [cm^2 s^{-1}], was estimated using the Wilke–Chang equation, shown in Equation (12) [35]:

$$D = \frac{7.4 \times 10^{-8}\, T\sqrt{\gamma M}}{\mu {V_m}^{0.6}} \tag{12}$$

In Equation (12), T [K] is the absolute temperature, M [g mol^{-1}] is the molar mass of the solvent, μ [mPa s] is the viscosity of the solvent, and V_m [cm^3 mol^{-1}] is the molecular volume of the solute at its normal boiling point. In the present study, V_m was approximated by the molar volume.

2.9. Effective Diffusion Coefficient for Molecules with Different Charge States in the Membrane

To investigate the influence of molecular charge state, systematically controlled by solution pH, on membrane permeability, membrane permeation experiments were performed using Methyl Orange as an anionic/neutral pH-responsive model compound, following the procedure described in Section 2.8. The effective diffusion coefficient in the membrane, D_{eff}, was evaluated under different pH conditions and compared with the values obtained under unbuffered pure water conditions.

Methyl Orange solutions were prepared by dissolving the dye at a concentration of 1 mM in Britton–Robinson buffer solutions with pH values of 2, 7, and 12, which were used in place of pure water in the permeation experiments described in Section 2.8. Prior to the permeation tests, Methyl Orange solutions with a concentration of 10 μM were prepared in Britton–Robinson buffer at pH 2, 7, and 12, and their UV-visible absorption spectra were measured to determine the isosbestic point and the absorption maximum wavelength at each pH. For the membrane permeation experiments, 250 mL of the 1 mM Methyl Orange solution at each pH was introduced into the feed side of the glass permeation cell, while 250 mL of the corresponding Britton–Robinson buffer solution at the same pH was placed on the permeate side. The concentration of the feed-side solution at t = 0 s and the concentration of the permeate-side solution at each sampling time were determined using calibration curves prepared in advance at the isosbestic point. The effective diffusion coefficient D_{eff} was calculated from the concentration profiles and the average membrane thickness and was compared with the corresponding values obtained under pure water conditions. After completion of each experiment, the pH values of both the feed and permeate solutions were measured to confirm pH stability during permeation.

Similar experiments were conducted using Neutral Red as a cationic/neutral pH-responsive model molecule. Britton–Robinson buffer solutions with pH values of 2, 7, and 12 were prepared, and UV-visible absorption spectra were recorded to determine the absorption maximum wavelength. Neutral Red solutions with a concentration of 1 mM were then subjected to membrane permeation experiments under the same conditions as those used for Methyl Orange. Concentrations were determined using calibration curves prepared in advance at the absorption maximum wavelength. The effective diffusion coefficient D_{eff} was calculated. The pH values of both the feed and permeate solutions

were measured after each experiment to verify the absence of significant pH drift across the membrane.

3. Results and Discussion

3.1. Preparation of KGM Free-Standing Membranes

Drying 1 wt% aqueous KGM solution cast in a glass Petri dish resulted in the formation of continuous, film-like KGM layer that adhered firmly to the hydrophilic glass surface. The strong adhesion is attributed to hydrogen bonding interactions between the hydroxyl-rich KGM chains and the glass substrate. In contrast, upon the addition of an aqueous alkaline solution (KOH), the KGM did not dissolve; instead, a transparent, self-supporting membrane was obtained that could be readily detached from the Petri dish. The alkaline-induced insolubilization of KGM proceeded rapidly, yielding a membrane-shaped product that retained the macroscopic morphology of the original dried film.

The resulting membrane remained insoluble during subsequent washing in pure water and treatment in hot water, indicating successful conversion of the water-soluble KGM into a water-insoluble network structure, while maintaining its original form without noticeable deformation. Furthermore, after the hot-water treatment, the membrane exhibited an apparent increase in mechanical rigidity accompanied by enhanced elastic recovery upon manual bending, suggesting further stabilization of the internal polymer network. The appearance of the obtained membrane is shown in Figure 3a. The membrane was colorless and transparent, and its surface was smooth without visible defects or macroscopic inhomogeneities. The uniform appearance across the entire membrane area indicates good macroscopic homogeneity and suggests that the film was formed as a continuous and uniform polymer layer during the casting and insolubilization processes. In addition, the membrane retained its macroscopic appearance even after long-term storage in pure water, indicating good structural stability under aqueous conditions. A representative photograph of such a membrane is provided in the Supporting Information. This interpretation was further supported by quantitative thickness measurements. The average thickness of five independently prepared membranes was 153 μm, with a standard deviation of 13.6 μm. For each membrane, the thickness value was determined as the average of measurements taken at 10 different positions on the membrane surface. The coefficient of variation, calculated from the standard deviation and mean thickness for these 10 measurement points, averaged 12.9% across the five membranes. These results indicate that the prepared KGM membranes exhibited reasonably good thickness reproducibility and within-membrane uniformity.

3.2. Characterization of KGM Free-Standing Membranes

The membrane surface was smooth, exhibiting no noticeable roughness or topographical irregularities. In contrast, the internal structure of the membrane warrants closer examination. Although direct observation of the membrane in the hydrated state is difficult, cross-sectional analysis of dried membranes provides valuable structural information at the micrometer scale and can be readily performed using SEM. Figure 3b presents a cross-sectional SEM image of the obtained membrane.

The image demonstrates that the membrane has a dense and homogeneous internal structure throughout the entire thickness, with no observable macropores, voids, or defects. Furthermore, no signs of partial delamination or layered separation were detected within the cross section. This observation indicates that the membrane forms a continuous polymer phase rather than a macroporous network at the resolution of SEM, which is consistent with the absence of detectable pressure-driven pure-water permeation, as discussed in the following sections. In addition, the surface SEM image shown in Figure 3c confirms that the membrane surface is smooth and free from observable defects or pores at the micrometer

scale. Taken together, Figure 3a,c indicates that the membrane surface is homogeneous at both the macroscopic and microscopic levels.

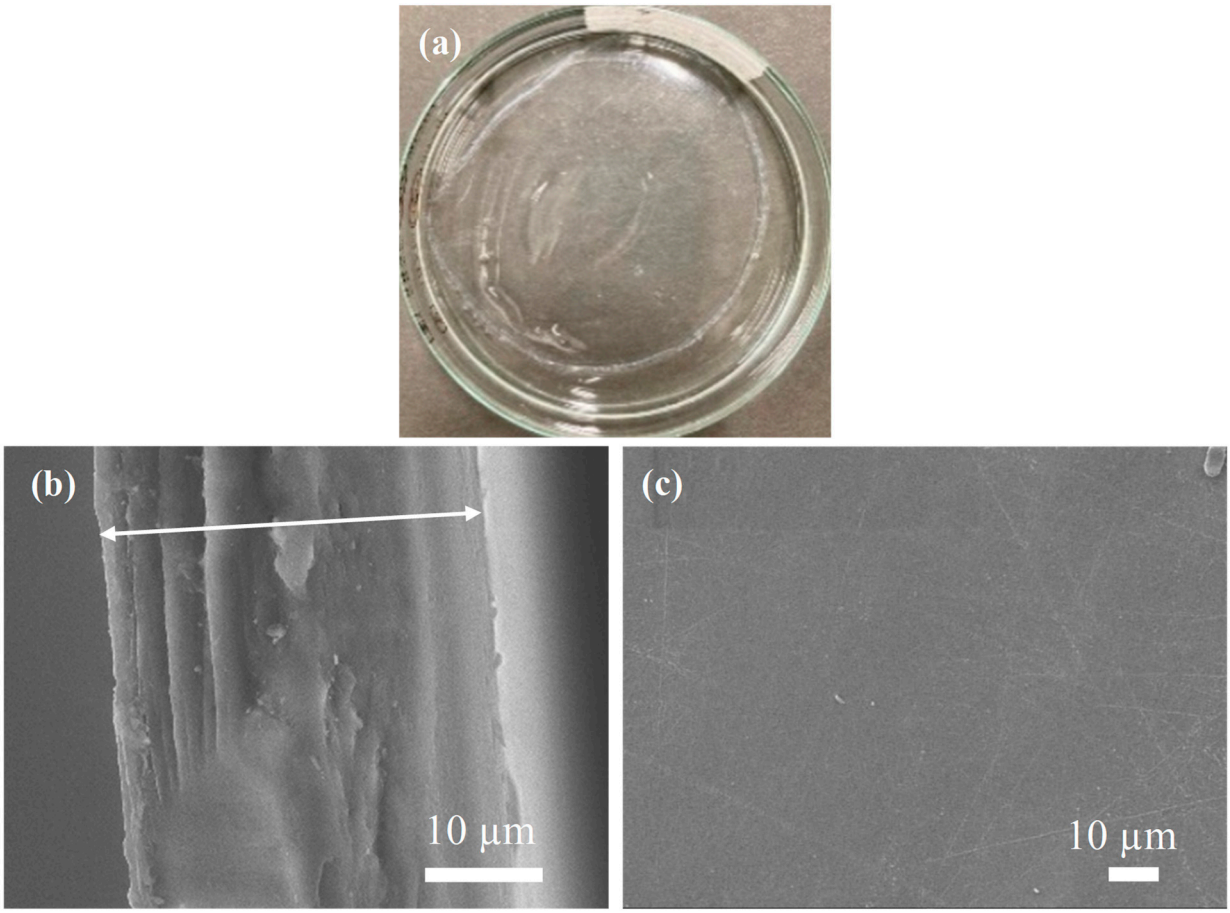


Figure 3. (**a**) Photograph of the KGM free-standing membrane. (**b**) Cross-sectional scanning electron microscopy (SEM) image of the membrane, with the arrow indicates the membrane region. (**c**) Surface SEM image of the membrane.

Furthermore, infrared absorption spectroscopy revealed clear differences in the spectral features of KGM before and after insolubilization. Figure 4 shows the ATR–FT-IR spectra of KGM free-standing membrane obtained before and after alkaline insolubilization.

The overall spectral features of KGM before treatment were in good agreement with those previously reported by Ye et al. [36]. The broad absorption band around 3340 cm^{-1} is attributed to O-H stretching vibrations, while the peak at approximately 2880 cm^{-1} corresponds to C-H stretching vibrations of the methyl groups in KGM. The absorption band near 1640 cm^{-1} is associated with hydrogen-bonded water and intermolecular hydrogen bonding, whereas the peak at approximately 1725 cm^{-1} is assigned to the C=O stretching vibration of acetyl groups. These peaks confirm the characteristic structural features of KGM prior to insolubilization.

In contrast, in the spectrum of the insolubilized KGM free-standing membrane, the absorption band near 1640 cm^{-1} remained, whereas the acetyl-related peak at 1725 cm^{-1} was no longer observed. The disappearance of this peak provides clear spectroscopic evidence for deacetylation during alkaline treatment. This result indicates that although the original KGM contained acetylated residues, base-induced deacetylation occurred along the polymer backbone, leading to a modification of the polysaccharide structure. These observations suggest that the insolubilization of KGM is closely associated with base-induced deacetylation of acetyl groups along the polymer backbone. For reference, X-ray

diffraction patterns of the original KGM powder, a dried KGM film without insolubilization, and an alkali-insolubilized KGM film are provided in the Supporting Information. No sharp diffraction peaks were observed for any of these samples, suggesting that neither film formation nor alkaline insolubilization induced pronounced crystallization of KGM under the present conditions.

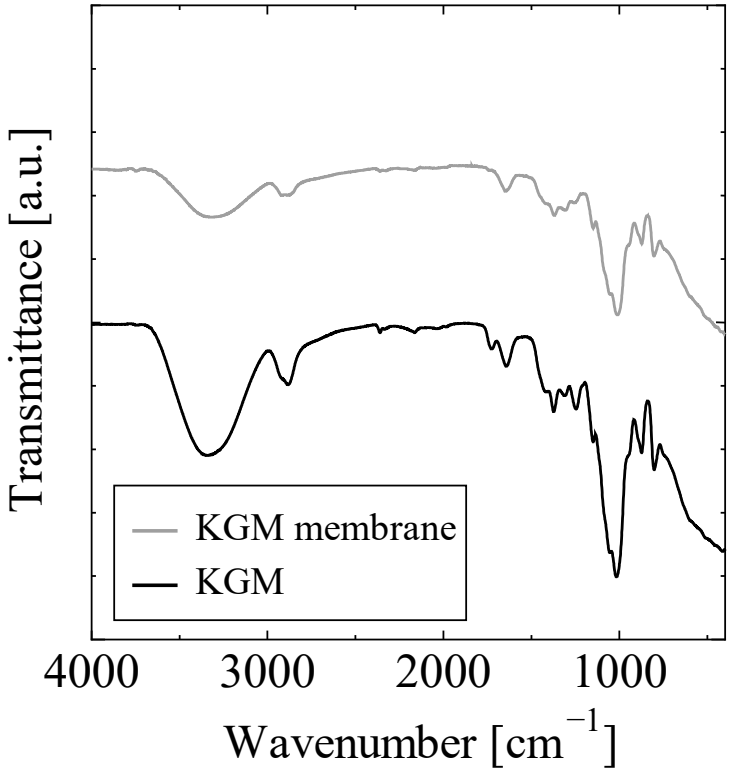


Figure 4. Infrared absorption spectra of pristine KGM and the KGM free-standing membrane.

3.3. Mechanical Properties Test

The KGM free-standing membrane did not fracture or disintegrate during cutting and could be successfully punched into dumbbell-shaped specimens, demonstrating sufficient mechanical integrity for tensile testing. To evaluate the mechanical strength of the KGM membrane, tensile tests were performed. For comparison, PVDC and RC films were prepared in the same specimen geometry and subjected to identical tensile testing conditions.

The maximum tensile strength and tensile strain of the KGM free-standing membranes, PVDC, and RC under both dry and wet conditions are shown in Figures 5 and 6, respectively. For each condition, ten specimens (n = 10) were tested. The error bars in these figures represent twice the standard deviation, reflecting the variability among the specimens.

For the KGM free-standing membrane, the maximum tensile strength was 57.9 MPa in the dry state and 1.4 MPa in the wet state, while the corresponding tensile strain values were 15.8% (dry) and 175.5% (wet). For comparison, it has been reported that KGM films cast from a 1.0 wt% aqueous solution onto polystyrene substrates exhibit a tensile strength of approximately 80 MPa and a tensile strain of about 33% [36]. Although the values obtained in the present study are somewhat lower, the KGM free-standing membranes nevertheless exhibit relatively high tensile strength in the dry state among polysaccharide-based membranes.

In contrast, films prepared by dispersing KGM powder in calcium hydroxide solutions with glycerol added as a plasticizer have been reported to show much lower tensile strengths of 0.77–1.19 MPa and tensile strains of approximately 12.0% [37]. This pronounced difference highlights the strong influence of membrane preparation routes and plasticizer

incorporation on the mechanical properties of KGM-based materials, and underscores the effectiveness of the present insolubilization approach in producing mechanically robust membranes without plasticizers.

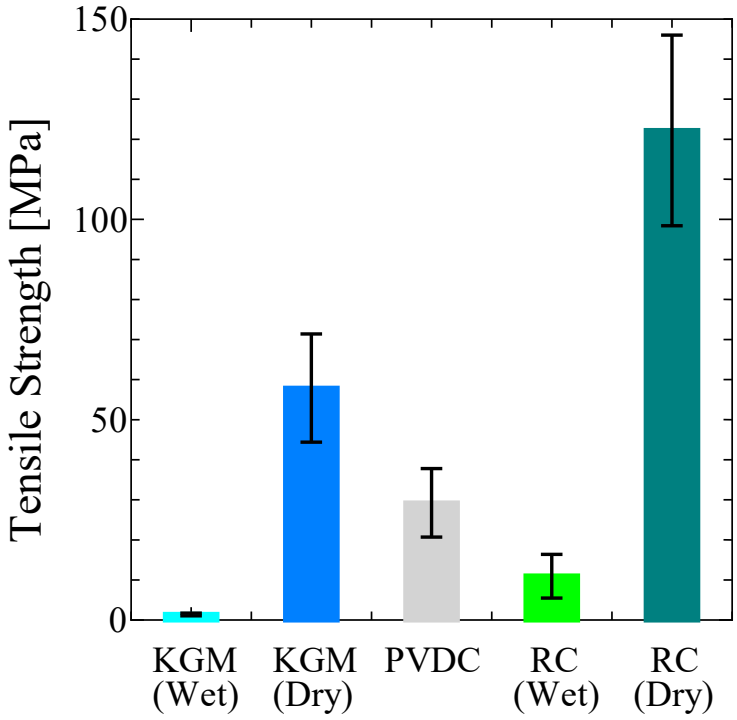


Figure 5. Tensile strength of the KGM free-standing membrane, polyvinylidene chloride (PVDC), and regenerated cellulose (RC). Error bars represent ±2 standard deviations (n = 10).

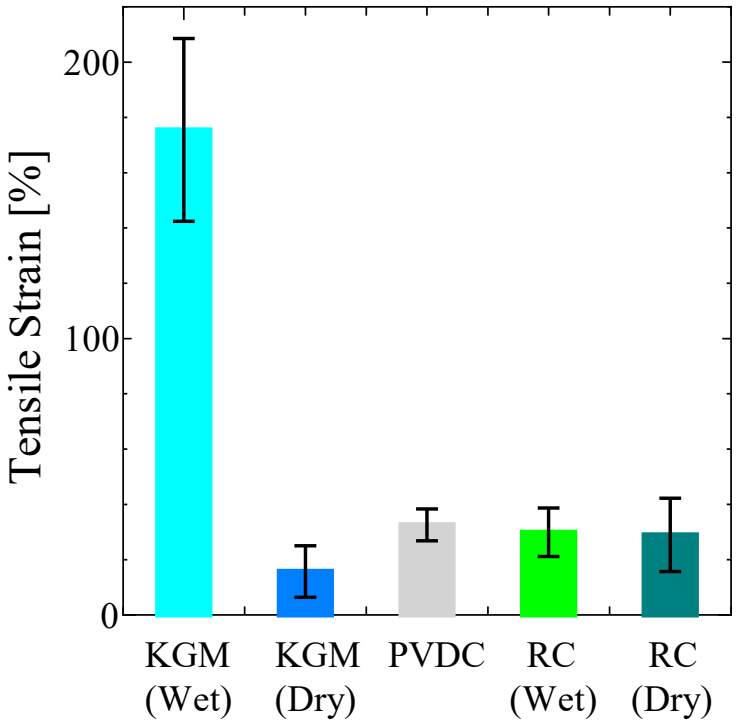


Figure 6. Tensile strain of KGM free-standing membrane, polyvinylidene chloride (PVDC), and regenerated cellulose (RC). Error bars represent ±2 standard deviations (n = 10).

The tensile properties obtained in this study are also broadly consistent with literature values for the reference materials. Xiong et al. reported dry and wet tensile strengths of approximately 94 MPa and 20 MPa, respectively, for RC films [38], while PVDC films typically exhibit a tensile strength of around 26 MPa and a tensile strain of approximately 20% [39]. Furthermore, according to Perera et al., the tensile strengths of many polysaccharide-based films are generally below 40 MPa [40].

Based on these comparisons, the KGM free-standing membranes prepared in this study can be regarded as exhibiting comparatively high tensile strength among polysaccharide-based membranes, particularly in the dry state. These results suggest that the preparation procedure described in Section 2.2 promotes the formation of a dense polymer network stabilized by strong intermolecular hydrogen bonding. Although the tensile strength of the KGM membrane is lower than that of RC, the membrane retains sufficient mechanical integrity in the hydrated state for use as a separation membrane, while simultaneously exhibiting exceptionally high flexibility. This combination of mechanical robustness in the dry state and pronounced flexibility in the wet state represents a key advantage for the practical application of KGM free-standing membranes in membrane separation processes.

3.4. Determination of Water Vapor Permeability (WVP)

The mass of the water vapor permeability cup equipped with the prepared KGM free-standing membrane was recorded at 10 min intervals over a period of 2 h. Figure 7 shows the increase in mass, Δw [kg], relative to the initial mass w_0 [kg] as a function of elapsed time t [s]. The rate of moisture uptake, Δm, was determined from the slope of the linear region of the Δw versus t plots, and the WVP of each sample was subsequently calculated from this value, as shown in Figure 8. All measurements were performed using three independent specimens (n = 3). The error bars in Figures 7 and 8 represent twice the standard deviation, reflecting the experimental variability among the samples.

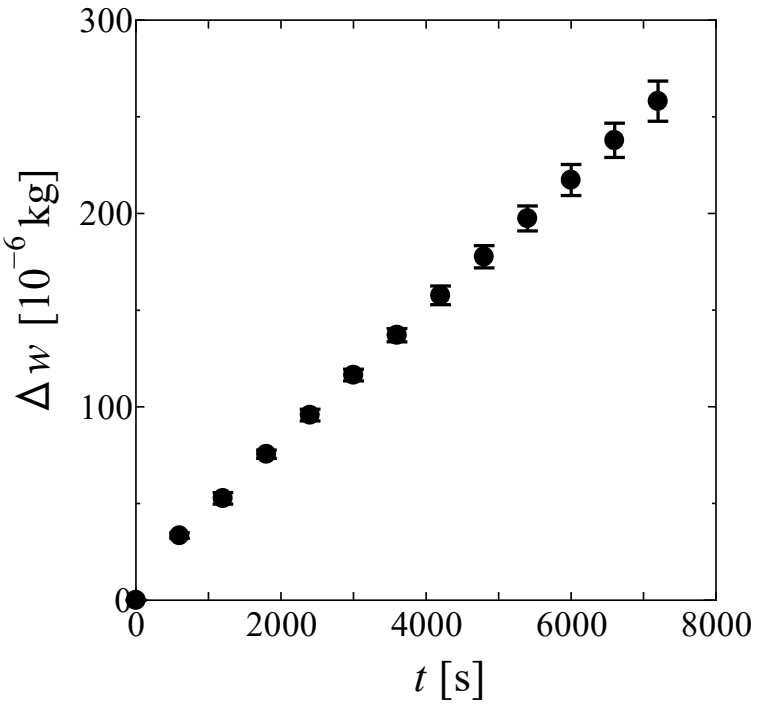


Figure 7. Increase in mass (Δw) relative to initial mass (w_0) as a function of elapsed time (t) for the KGM free-standing membrane. Measurements were performed in triplicate (n = 3).

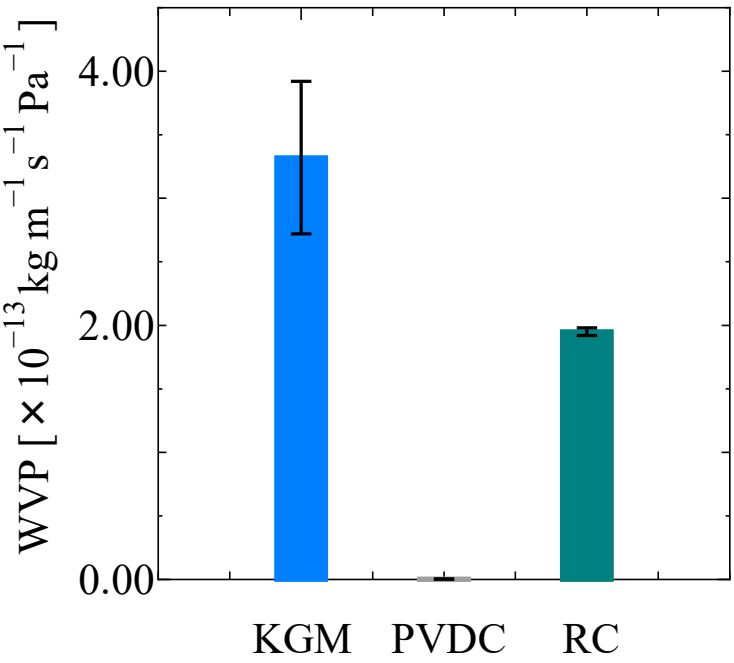


Figure 8. Water vapor permeability (WVP) of the KGM free-standing membrane, PVDC film, and RC film. Measurements were performed in triplicate (n = 3).

The WVP of the KGM free-standing membranes was determined to be 3.32×10^{-13} kg m^{-1} s^{-1} Pa^{-1}. For comparison, the WVP values of PVDC and RC were 3.84×10^{-16} and 1.95×10^{-13} kg m^{-1} s^{-1} Pa^{-1}, respectively.

These values are in good agreement with previously reported data. Wu et al. reported a WVP of 1.82×10^{-13} kg m^{-1} s^{-1} Pa^{-1} for pure KGM films [24], while Wei et al. obtained a value of 3.355×10^{-13} kg m^{-1} s^{-1} Pa^{-1} for deacetylated KGM membranes measured at 38 °C [41]. Similarly, Shellhammer et al. reported WVP values of 2.22×10^{-16} kg m^{-1} s^{-1} Pa^{-1} for PVDC and 0.84×10^{-13} kg m^{-1} s^{-1} Pa^{-1} for cellophane (RC) [42].

Polysaccharides rich in hydroxyl (OH) groups generally exhibit high water vapor permeability, owing to strong interactions between water molecules and hydrophilic functional groups. The present results are consistent with this characteristic behavior and demonstrate that KGM free-standing membranes intrinsically possess high water vapor permeability. Although a high WVP can be disadvantageous for applications requiring moisture barrier performance, it also serves as an important indicator of strong membrane–water interactions and high molecular transport capability under hydrated conditions. Therefore, to assess the suitability of the KGM membranes for separation applications in the wet state, pressure-driven pure-water permeability and solute permeation behavior were further investigated, as described in Sections 2.7 and 2.8.

3.5. Resistance to Organic Solvents

Resistance to organic solvents is an essential requirement for membrane materials intended for practical separation processes, particularly when exposure to non-aqueous environments or solvent-containing streams is anticipated. For polysaccharide-based membranes, solvent resistance is also a key indicator of successful insolubilization and network formation, as insufficiently stabilized membranes may swell, dissolve, or leach polymer components when contacted with organic solvents. Therefore, evaluating the stability of the KGM free-standing membranes against representative organic solvents

provides important insight into their structural integrity and potential applicability beyond purely aqueous systems.

Table 1 summarizes the mass and thickness of the KGM free-standing membranes after immersion in acetone and *n*-hexane for 0, 30, 60, and 1440 min. No significant changes in either mass or thickness were observed throughout the immersion period. This behavior is consistent with the general characteristic that many biopolymers are insoluble in common organic solvents [43,44]. The absence of measurable changes indicates that solvent-induced swelling did not occur in either polar (acetone) or nonpolar (*n*-hexane) environments. This observation also suggests that the internal polymer network structure remained stable during solvent exposure and that the free volume within the membrane was not significantly altered by immersion in these solvents. Furthermore, the membranes exhibited excellent resistance to organic solvents, with no visible signs of dissolution, deformation, or component leaching into either solvent. These results demonstrate that the alkaline insolubilization treatment effectively stabilizes the KGM membrane structure, enabling it to maintain dimensional and mass stability even under prolonged exposure to organic solvents.

Table 1. Changes in film thickness and mass of KGM free-standing membranes after immersion in acetone and *n*-hexane.

Acetone						
Elapsed Time [min]	**Mass [g]**			**Film Thickness [mm]**		
	Run 1	**Run 2**	**Run 3**	**Run 1**	**Run 2**	**Run 3**
0	0.0103	0.0085	0.0129	0.0362 ± 0.0120	0.0325 ± 0.0017	0.0607 ± 0.0219
30	0.0101	0.0083	0.0124	0.0358 ± 0.0120	0.0303 ± 0.0010	0.0680 ± 0.0144
60	0.0109	0.0090	0.0125	0.0357 ± 0.0110	0.0350 ± 0.0044	0.0582 ± 0.0131
120	0.0096	0.0081	0.0118	0.0407 ± 0.0040	0.0360 ± 0.0020	0.0515 ± 0.0050
n-Hexane						
Elapsed Time [min]	Mass [g]			Film Thickness [mm]		
	Run 1	Run 2	Run 3	Run 1	Run 2	Run 3
0	0.0091	0.0110	0.0107	0.0339 ± 0.0095	0.0420 ± 0.0131	0.0491 ± 0.0185
30	0.0092	0.0110	0.0108	0.0380 ± 0.0165	0.0438 ± 0.0194	0.0505 ± 0.0048
60	0.0092	0.0112	0.0110	0.0360 ± 0.0105	0.0423 ± 0.0162	0.0373 ± 0.0078
120	0.0092	0.0118	0.0109	0.0302 ± 0.0038	0.0341 ± 0.0033	0.0290 ± 0.0056

3.6. Evaluation of Pure Water Permeability and Estimation of Effective Size of Water Permeation Channels

To estimate the effective size of the water permeation channels, expressed as the hydraulic channel radius, in the prepared KGM free-standing membranes, their pure water permeability was examined under pressure-driven conditions. Pure water permeation tests are commonly employed to evaluate convective transport through membrane channels and to provide indirect insight into channel structure and overall structural compactness. Even when measurable permeation is not observed, such experiments can provide an upper-limit estimate of the size of possible transport channels within the membrane.

For the KGM free-standing membranes, the mass of permeated water, w_p [kg], was monitored while the operating pressure Δp [MPa] was increased stepwise from 0.050 to 0.25 MPa at 30 min intervals. Under all tested conditions, the measured w_p remained at 0 kg, indicating that no visible water droplets were observed at the permeate outlet and no detectable pressure-driven water permeation occurred through the membranes within the investigated pressure range. This observation suggests that continuous channels capable of sustaining convective water flow are absent or extremely small within the membrane

structure. Since actual measurements were not available, the permeation flow rate was estimated based on the detection limit defined by the absence of droplet formation at the permeate outlet.

Based on the experimental observation that not a single water droplet was released from the permeate side during the measurement period, the permeated water mass was assumed to be lower than the typical mass of one water droplet. Accordingly, the upper detection limit of the permeated mass was conservatively estimated to be $\leq$0.05 g over a period of 10 min at Δp = 0.25 MPa. Using this upper-limit permeation rate, the filtration coefficient was estimated using Equation (4). An effective permeation area $A = 4.15 \times 10^{-4}$ m^2, a water density of 998.2 kg m^{-3}, the film thickness L =1.08 $\times$ 10^{-4} m, and the viscosity of the permeate $\eta = 8.90 \times 10^{-4}$ Pa s were used to estimate the void fraction of the membrane ε and the filtration coefficient K_F [32]. Based on these conservative assumptions, the mean channel size r was calculated to be $\leq$3.1 nm.

These results demonstrate that the KGM free-standing membranes exhibit extremely low hydraulic permeability and effectively suppress convective water transport. This behavior suggests that the membranes possess a highly compact internal structure without continuous channels large enough to sustain pressure-driven water flow. Therefore, the present result provides an upper-limit estimate for the possible transport channel size and supports the interpretation that molecular transport through the membrane occurs predominantly via diffusion within a dense hydrated polymer network. Such structural compactness is likely attributable to a tightly packed polymer network stabilized by extensive intermolecular hydrogen bonding among the abundant hydroxyl groups along the KGM chains.

It is possible that measurable water permeation could be observed under higher operating pressures than those applied in the present study. However, in the current experimental setup, the accessible pressure range was limited, and investigation of pure water permeability under higher pressures is beyond the scope of the present work and remains an important subject for future studies.

3.7. Effective Diffusion Coefficient of Molecules in the Membrane

This section focuses on elucidating the size-dependent diffusion behavior of solute molecules within the dense KGM free-standing membrane, which represents a central outcome of this study. After determining the solute concentrations on the permeate side, the overall mass transfer coefficient K_{OL} was calculated based on Equation (10). By plotting the left-hand side of Equation (10) against the elapsed time t, highly linear relationships were obtained for all eight model molecules, as shown in Figure 9a–e.

The excellent linearity observed for all solutes indicates that the permeation process proceeded in a steady and reproducible manner, and suggests that effects such as membrane fouling, clogging, or time-dependent structural changes did not significantly influence the transport behavior during the measurements. The slope of each fitted straight line corresponds to $-2A\,K_{OL}/V$. By substituting the effective membrane area ($A = 2.38 \times 10^{-3}$ m^2) and the solution volume ($V = 2.5 \times 10^{-4}$ m^3), K_{OL} values were obtained for each solute.

At a stirring speed of 900 rpm, the Reynolds number exceeded 10,000, indicating sufficiently turbulent flow conditions. Under such conditions, external mass transfer resistances in the liquid boundary layers on both the feed and permeate sides can be neglected, and the overall mass transfer coefficient K_{OL} can be approximated as the intramembrane mass transfer coefficient k_M. The effective diffusion coefficient within the membrane, D_{eff}, was therefore determined by multiplying k_M by the membrane thickness.

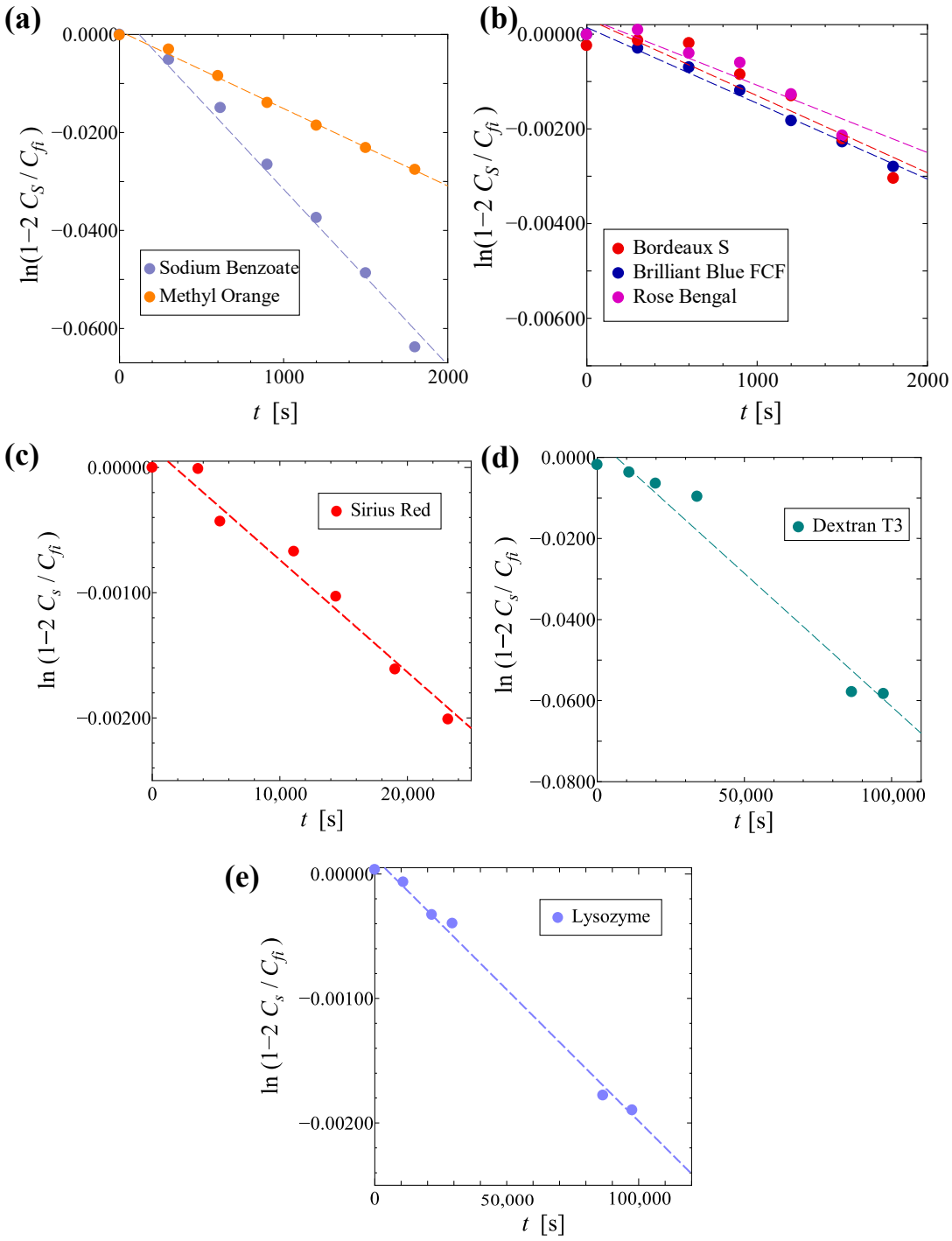


Figure 9. Time course of $\ln(1 - 2C_S/C_{fi})$ for eight model molecules at 25 °C. (**a**) M = 144.1 Da (sodium benzoate) and 327.4 Da (methyl orange). (**b**) M = 604.5 Da (Bordeaux S), 792.9 Da (Brilliant Blue FCF), and 1018 Da (Rose Bengal). (**c**) M = 1373 Da (Sirius Red). (**d**) M = 3000 Da (Dextran T3). (**e**) M = 14,600 Da (lysozyme).

Figure 10 shows the relationship between D_{eff} and the molecular weight M for the KGM free-standing membranes. For comparison, the diffusion coefficient in bulk water, D, estimated using the Wilke–Chang equation [35], is also shown. Over a molecular weight range spanning more than two orders of magnitude, the bulk diffusion coefficient D varied by only approximately eightfold, reflecting the weak molecular-weight dependence of diffusion in free aqueous solution. In sharp contrast, the effective diffusion coefficient D_{eff}

within the KGM membrane decreased by nearly three orders of magnitude (approximately 2000-fold) over the same molecular weight range.

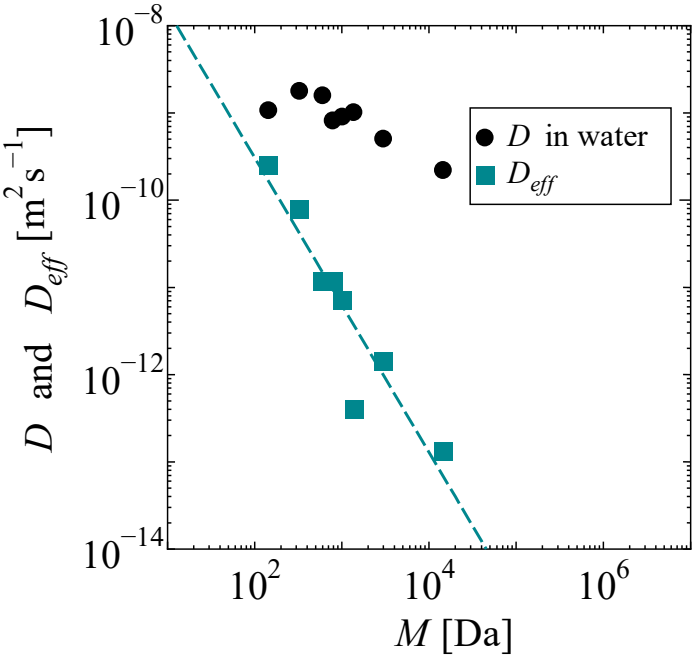


Figure 10. Effective diffusion coefficient (D_{eff}) of eight model molecules in KGM free-standing membranes at 25 °C. The diffusion coefficients in water (D) were estimated using the Wilke–Chang equation.

This pronounced difference demonstrates that mass transport within the KGM membrane is not governed by free diffusion in water, but is instead strongly constrained by the polymer network structure of the membrane. A clear power-law relationship, D_{eff} followed a power-law relationship with molecular weight M ($D_{eff} \propto M^{-1.7}$), was observed, indicating strong size-dependent hindrance of molecular diffusion within the membrane.

For comparison, Kashima et al. reported that calcium-crosslinked alginate membranes with a guluronic acid fraction of 0.56 exhibited a sharp decrease in D_{eff} from 2.20×10^{-12} to 2.01×10^{-14} m^2 s^{-1} as M increased from 180 to 504 Da, corresponding to a 109-fold reduction in D_{eff} for only a 2.8-fold increase in molecular weight [16]. Although the KGM free-standing membranes prepared in the present study do not show such an abrupt molecular-weight cutoff in the low-molecular-weight region, D_{eff} nevertheless decreases continuously and markedly with increasing molecular weight.

Taken together with the absence of detectable pure water permeation and the dense, nonporous morphology observed by SEM, these results indicate that molecular transport through the KGM membrane occurs predominantly via diffusion within a hydrated polymer network rather than via pressure-driven transport through well-defined pores. Pressure-driven permeation requires continuous pores large enough to sustain convective flow of bulk water. The absence of measurable pure-water permeation therefore indicates that such continuous channels are not present in the membrane within the investigated pressure range.

Nevertheless, solute molecules can still migrate through the membrane by diffusing through transient free volume and intermolecular spacing within the hydrated polysaccharide network. This transport behavior is consistent with a solution–diffusion mechanism commonly observed in dense polymer membranes. In such dense polymer membranes, molecular transport occurs through transient free volume within the polymer network rather than through permanent pores. Therefore, a well-defined pore radius is generally not an appropriate descriptor of the transport mechanism. This behavior enables molecular

fractionation based on differences in diffusion rates rather than on channel-size exclusion, suggesting that KGM free-standing membranes function as diffusion-selective separation media governed by hydrogen-bonded polysaccharide networks.

In addition, the stability of the membrane during diffusion measurements provides indirect evidence of its structural robustness. The diffusion experiments were conducted for extended periods approaching 10^5 s (approximately 28 h) while both compartments of the diffusion cell were vigorously stirred using turbine impellers rotating at 900 rpm. Under such conditions, turbulent flow is generated in close proximity to the membrane surface, subjecting the membrane to continuous hydrodynamic agitation. Despite these demanding conditions, the KGM membranes remained intact and exhibited stable diffusion behavior throughout the measurements, as evidenced by the excellent linearity of the concentration–time relationships shown in Figure 9. These observations indicate that the membrane structure remains mechanically and structurally stable during long-term diffusion experiments, further supporting the reliability of the measured diffusion-controlled transport behavior.

3.8. Effect of Molecular Charge State on Diffusion Within the Membrane

Methyl Orange (molecular weight: 327.4 Da) exists as a formally neutral molecule at pH $\leq$ 3.1 and as a monovalent anion at pH $\geq$ 4.4. Conversely, Neutral Red (molecular weight: 288.8 Da) becomes a monovalent cation at pH $\leq$ 6.8 and a neutral molecule at pH $\geq$ 8.0. Owing to their comparable molecular weights but different charge behaviors as a function of pH, these two dyes were used to investigate the effect of the charge state on their diffusion behavior within the KGM free-standing membrane by varying the pH.

The absorption spectra of Methyl Orange and Neutral Red at various pH values are shown in Figures 11a and 11b, respectively. In both cases, pronounced spectral changes were observed with changing pH, while clear isosbestic points were maintained. This behavior indicates reversible protonation and deprotonation equilibria of the dye molecules, confirming that their charge states change systematically with pH.

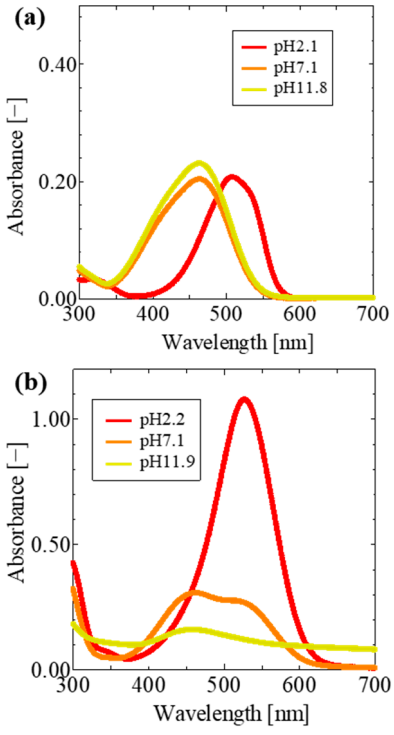


Figure 11. Absorption spectrum of Methyl Orange and Neutral Red in pH-adjusted solutions. (**a**) Methyl Orange. (**b**) Neutral Red. The Britton–Robinson buffer was used for pH adjustment.

Figure 12a,b shows the relationship between the effective diffusion coefficient D_{eff} and molecular weight within the KGM free-standing membrane, obtained by varying the pH of the Methyl Orange and neutral red solutions, respectively. In addition, the pH values of both the feed and permeate compartments before and after the experiments are summarized in Table 2.

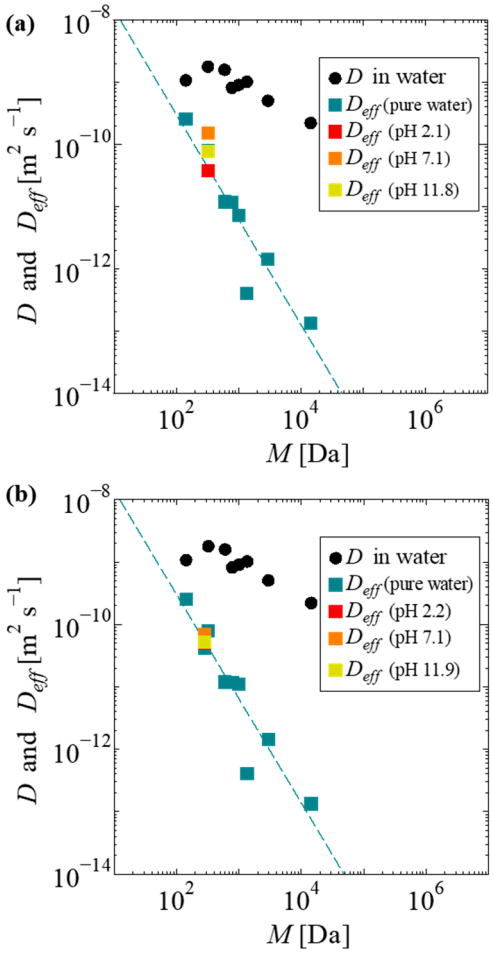


Figure 12. Effective diffusion coefficient (D_{eff}) of Methyl Orange and Neutral Red at different pH values. (**a**) Methyl Orange. (**b**) Neutral Red. The Britton–Robinson buffer was used for pH adjustment.

Table 2. pH values of Methyl Orange and Neutral Red solutions before and after permeation experiments in the mass-transfer cells.

Solute	**Methyl Orange**					
pH	**2.1**		**7.1**		**11.8**	
	Feed Side	**Stripping Side**	**Feed Side**	**Stripping Side**	**Feed Side**	**Stripping Side**
Before	2.14	2.14	7.07	7.07	11.83	11.83
After	2.19	2.22	6.76	6.98	11.96	11.94
Solute	Neutral Red					
pH	2.1		7.1		11.8	
	Feed side	Stripping side	Feed side	Stripping side	Feed side	Stripping side
Before	2.17	2.17	7.12	7.12	11.92	11.92
After	2.15	2.16	7.05	7.11	11.94	11.94

Figure 12a indicates that changes in pH, and thus the charge state of Methyl Orange, had no significant impact on its D_{eff}. Similarly, the D_{eff} of Neutral Red remained nearly constant regardless of pH (Figure 12b). Furthermore, Table 2 confirms that no measurable pH changes occurred between the two compartments separated by the KGM membrane during the measurements, indicating negligible proton transport across the membrane. No visible changes in the physical appearance or integrity of the membrane were observed across the pH range from 2 to 12.

A comparison of the D_{eff} values shows that Methyl Orange at pH 12 (formally bearing a -1 charge) and Neutral Red at pH 2 (formally bearing a +1 charge) exhibit nearly identical diffusion coefficients. This suggests that the permeation behavior of the KGM membrane for molecules with ± 1 formal charge is largely independent of their charge state, which is likely attributable to the neutral nature of KGM as a polysaccharide lacking ionizable functional groups capable of strong electrostatic interactions with solutes.

KGM is primarily composed of β-1,4-linked D-mannose and D-glucose units, whose dominant functional groups are hydroxyl groups along the polysaccharide backbone. Native KGM contains acetyl substituents at a frequency of approximately one per 9–19 sugar residues [19–21]; however, these groups are electrically neutral and are largely removed during the alkaline treatment used for membrane preparation. Consequently, the resulting membrane matrix remains essentially nonionic over the investigated pH range. Because KGM does not contain strongly ionizable functionalities such as carboxylate or amino groups, the membrane charge is expected to remain minimal even when the pH of the surrounding solution is varied. In addition, no obvious adsorption of the dye molecules onto the membrane was visually observed during the permeation experiments, which is qualitatively consistent with limited membrane–solute electrostatic interactions under the investigated conditions.

These findings demonstrate that the KGM free-standing membranes remain stable across a wide pH range (2–12) and that their separation performance depends primarily on molecular weight or size rather than the charge state of the solutes. Such charge-insensitive behavior is highly advantageous, as it enables size-based molecular fractionation while providing a chemically inert and non-interfering membrane matrix. Taken together, the chemical structure of KGM, the deacetylated nonionic membrane network, and the experimentally observed charge-independent diffusion behavior all support the conclusion that electrostatic interactions play only a minor role in the present transport system. This neutrality further suggests that KGM membranes can be combined with other functional materials or surface modifications without compromising their intrinsic separation performance. Within the investigated pH range, no visible changes in membrane appearance or integrity were observed during the permeation experiments, indicating that the membrane remained macroscopically stable under the examined conditions. Further investigation of pH-dependent changes in membrane properties, including surface morphology and mechanical behavior, remains an important subject for future study.

3.9. Comparison with Previously Reported Biopolymer Membranes

To place the present results in the context of previously reported biopolymer-based membranes, representative membrane systems and their transport characteristics are summarized in Table 3. Previous studies on polysaccharide-based membranes have primarily focused on pressure-driven separation processes such as nanofiltration. In contrast, the KGM membrane investigated in this study exhibits diffusion-controlled transport through a dense hydrogen-bonded polymer network without measurable pressure-driven water permeation. Notably, the present system enables systematic evaluation of diffusion-controlled transport over a relatively wide molecular-weight range (144–14,600 Da).

Table 3. Comparison of representative polysaccharide-based membranes reported in the literature.

Membrane Material	Polymer Type	Transport Mechanism	Molecular Weight Range Investigated	Reference
Calcium alginate membrane	Anionic polysaccharide	Diffusion-controlled transport in swollen polymer network	180–1370 Da	Kashima et al. [18]
Agarose-natural rubber latex IPN membrane	Neutral polysaccharide/natural polyisoprene elastomer	Pressure-driven nanofiltration	227–623 Da	Cavalcante et al. [45]
Cellulose–chitosan membrane	Neutral/cationic polysaccharide blend	Pressure-driven organic solvent nanofiltration	236–1017 Da	Hardian et al. [46]
KGM membrane (this work)	Neutral polysaccharide	Diffusion-controlled transport in hydrogen-bonded polymer network	144–14,600 Da	This work.

4. Conclusions

In this study, KGM free-standing membranes were successfully prepared via a base-induced insolubilization process, and their structural, mechanical, and transport properties were systematically investigated. FT-IR analysis confirmed that the insolubilization originates from the deacetylation of KGM chains, which promotes the formation of a densely hydrogen-bonded polymer network stabilized by extensive intermolecular hydrogen bonding. As a result, the membranes exhibited excellent mechanical stability, characterized by high tensile strength in the dry state and remarkable flexibility in the hydrated state.

Transport experiments revealed that the KGM membranes possess a highly compact internal structure, effectively suppressing the convective flow of pure water within the investigated pressure range. Mass transfer analyses using a series of model solutes demonstrated that the effective diffusion coefficient D_{eff} is predominantly governed by molecular size. Within the range of solute charge states examined in this study, no discernible influence of charge on D_{eff} was observed. In addition, the permeation behavior remained stable over a wide pH range (2–12), which is consistent with the neutral chemical nature of the KGM polysaccharide. KGM consists primarily of β-1,4-linked D-mannose and D-glucose units whose dominant functional groups are hydroxyl groups, and it lacks strongly ionizable groups such as carboxylate or amino groups that would introduce significant electrostatic interactions. Furthermore, the alkaline treatment used during membrane preparation promotes deacetylation of the native acetyl substituents, resulting in a polymer network that remains essentially nonionic under the investigated conditions.

Overall, these results indicate that KGM free-standing membranes enable molecular fractionation based on size-dependent diffusion within a hydrated polymer network, rather than sharp pore-size exclusion. The combination of high mechanical durability, pH stability, and minimal electrostatic interference under the investigated conditions highlights the potential of these membranes as diffusion-selective separation media for aqueous systems, and as a structurally stable, non-interacting matrix suitable for integration with functional components in composite membrane designs. Future work should address application-oriented membrane design and practical separation performance based on the fundamental findings obtained in this study. In addition, application-specific safety evaluations, including possible contamination, leaching behavior, and, where relevant, incorporation of antibacterial functionality, remain important subjects for future study. Application-specific safety evaluations, including possible contamination, leaching behav-

ior, and, where relevant, incorporation of antibacterial functionality, remain important subjects for future study.

Supplementary Materials: The following supporting information can be downloaded at https://www.mdpi.com/article/10.3390/polysaccharides7020043/s1, Table S1: Preparation conditions for KGM free-standing membranes; Figure S1: Average wet film thickness for samples No. 1 and 3–15. The measurements were performed in triplicate (n = 3), and the error bars represent twice the standard deviation, corresponding to a 95% confidence interval; Figure S2: Average moisture content of samples No. 1 and 3–15. The measurements were performed in triplicate (n = 3), and the error bars represent twice the standard deviation, corresponding to a 95% confidence interval; Figure S3: Representative photographs of KGM free-standing membranes stored in pure water: (a) within 1 h after alkaline treatment, (b) after 6 months of storage in pure water, and (c) after 9 months of storage in pure water. The membranes retained their macroscopic film shape during long-term storage under aqueous conditions; Figure S4: X-ray diffraction patterns of (a) the original KGM powder, (b) a dried KGM film without alkaline insolubilization treatment, and (c) a dried KGM film after alkaline insolubilization treatment with KOH.

Author Contributions: M.M. and M.H. performed the experiments and contributed to data collection and analysis. M.M. and M.H. curated and interpreted the data in collaboration with K.K., M.H. and K.K. conceived the study and supervised the research. M.M. drafted the manuscript. All authors have read and agreed to the published version of the manuscript.

Funding: This research was funded by the Japan Society for the Promotion of Science (JSPS) through its Grants-in-Aid for Scientific Research (KAKENHI; Nos. JP22H01631 and JP23H03577). This research was also supported by an industrial partner under a commissioned research agreement.

Data Availability Statement: The raw data supporting the conclusions of this article will be made available by the authors on request.

Acknowledgments: We gratefully acknowledge the financial support from the Japan Society for the Promotion of Science (JSPS) through its Grants-in-Aid for Scientific Research (KAKENHI; Nos. JP22H01631 and JP23H03577). We also thank Yutaro Chiba of the National Institute of Technology, Fukushima College for his technical support.

Conflicts of Interest: The authors received research funding from an industrial partner. The funder had no role in the design of the study, the analysis of the data, or the decision to publish. The authors declare no conflicts of interest associated with this manuscript.

Abbreviations

The following abbreviations are used in this manuscript:

KGM	Konjac glucomannan
PVDC	Polyvinylidene chloride
RC	Regenerated cellulose
WVP	Water vapor permeability
SEM	Scanning electron microscopy

References

1. Sahu, L.R.; Yadav, D.; Borah, D.; Gogoi, A.; Goswami, S.; Hazarika, G.; Karki, S.; Borpatra Gohain, M.; Sawake, S.V.; Jadhav, S.V.; et al. Polymeric Membranes for Liquid Separation: Innovations in Materials, Fabrication, and Industrial Applications. *Polymers* **2024**, *16*, 3240. [CrossRef] [PubMed]
2. Hatti-Kaul, R.; Nilsson, L.J.; Zhang, B.; Rehnberg, N.; Lundmark, S. Designing Biobased Recyclable Polymers for Plastics. *Trends Biotechnol.* **2020**, *38*, 50–67. [CrossRef]
3. Garavand, F.; Rouhi, M.; Razavi, S.H.; Cacciotti, I.; Mohammadi, R. Improving the Integrity of Natural Biopolymer Films Used in Food Packaging by Crosslinking Approach: A Review. *Int. J. Biol. Macromol.* **2017**, *104*, 687–707. [CrossRef]

4. Moore, C.J. Synthetic Polymers in the Marine Environment: A Rapidly Increasing, Long-Term Threat. *Environ. Res.* **2008**, *108*, 131–139. [CrossRef] [PubMed]
5. Gowthaman, N.S.K.; Lim, H.N.; Sreeraj, T.R.; Amalraj, A.; Gopi, S. Advantages of Biopolymers over Synthetic Polymers: Social, Economic, and Environmental Aspects. In *Biopolymers and Their Industrial Applications*; Elsevier: Amsterdam, The Netherlands, 2021; pp. 351–372. [CrossRef]
6. Jabeen, N.; Atif, M. Polysaccharides Based Biopolymers for Biomedical Applications: A Review. *Polym. Adv. Technol.* **2024**, *35*, e6203. [CrossRef]
7. Dassanayake, R.S.; Acharya, S.; Abidi, N.; Dassanayake, R.S.; Acharya, S.; Abidi, N. Biopolymer-Based Materials from Polysaccharides: Properties, Processing, Characterization and Sorption Applications. In *Advanced Sorption Process Applications*; IntechOpen: London, UK, 2018. [CrossRef]
8. Abdul Khalil, H.P.S.; Saurabh, C.K.; Tye, Y.Y.; Lai, T.K.; Easa, A.M.; Rosamah, E.; Fazita, M.R.N.; Syakir, M.I.; Adnan, A.S.; Fizree, H.M.; et al. Seaweed Based Sustainable Films and Composites for Food and Pharmaceutical Applications: A Review. *Renew. Sustain. Energy Rev.* **2017**, *77*, 353–362. [CrossRef]
9. Ramesh, H.P.; Tharanathan, R.N. Carbohydrates—The Renewable Raw Materials of High Biotechnological Value. *Crit. Rev. Biotechnol.* **2003**, *23*, 149–173. [CrossRef]
10. Nešić, A.; Cabrera-Barjas, G.; Dimitrijević-Branković, S.; Davidović, S.; Radovanović, N.; Delattre, C.; Nešić, A.; Cabrera-Barjas, G.; Dimitrijević-Branković, S.; Davidović, S.; et al. Prospect of Polysaccharide-Based Materials as Advanced Food Packaging. *Molecules* **2019**, *25*, 135. [CrossRef] [PubMed]
11. Wang, L.; Chen, C.; Wang, J.; Gardner, D.J.; Tajvidi, M. Cellulose Nanofibrils versus Cellulose Nanocrystals: Comparison of Performance in Flexible Multilayer Films for Packaging Applications. *Food Packag. Shelf Life* **2020**, *23*, 100464. [CrossRef]
12. Renkin, E.M. Filtration, Diffusion, and Molecular Sieving through Porous Cellulose Membranes. *J. Gen. Physiol.* **1954**, *38*, 225–243. [PubMed]
13. Hoenich, N. Cellulose for Medical Applications: Past, Present, and Future. *BioResources* **2006**, *1*, 270–280. [CrossRef]
14. Tang, H.; Chang, C.; Zhang, L. Efficient Adsorption of Hg^{2+} Ions on Chitin/Cellulose Composite Membranes Prepared via Environmentally Friendly Pathway. *Chem. Eng. J.* **2011**, *173*, 689–697. [CrossRef]
15. Yan, L.; Li, P.; Zhou, W.; Wang, Z.; Fan, X.; Chen, M.; Fang, Y.; Liu, H. Shrimp Shell-Inspired Antifouling Chitin Nanofibrous Membrane for Efficient Oil/Water Emulsion Separation with In Situ Removal of Heavy Metal Ions. *ACS Sustain. Chem. Eng.* **2019**, *7*, 2064–2072. [CrossRef]
16. Kashima, K.; Imai, M. Selective Diffusion of Glucose, Maltose, and Raffinose through Calcium Alginate Membranes Characterized by a Mass Fraction of Guluronate. *Food Bioprod. Process.* **2017**, *102*, 213–221. [CrossRef]
17. Kashima, K.; Inage, T.; Yamaguchi, Y.; Imai, M. Tailorable Regulation of Mass Transfer Channel in Environmentally Friendly Calcium Alginate Membrane for Dye Removal. *J. Environ. Chem. Eng.* **2021**, *9*, 105210. [CrossRef]
18. Yoshida, K.; Kashima, K. Nano-Structural Modification of Mass Transfer Channels in Alginate Membrane by Dispersed Oligoethylene Glycol for Nanofiltration Applications. *Colloid Polym. Sci.* **2025**, *303*, 1261–1271. [CrossRef]
19. Zhu, F. Modifications of Konjac Glucomannan for Diverse Applications. *Food Chem.* **2018**, *256*, 419–426. [CrossRef] [PubMed]
20. Sun, Y.; Xu, X.; Zhang, Q.; Zhang, D.; Xie, X.; Zhou, H.; Wu, Z.; Liu, R.; Pang, J. Review of Konjac Glucomannan Structure, Properties, Gelation Mechanism, and Application in Medical Biology. *Polymers* **2023**, *15*, 1852. [CrossRef]
21. Huang, R.; Qi, W.; Feng, L.; Su, R.; He, Z. Self-Assembling Peptide–Polysaccharide Hybrid Hydrogel as a Potential Carrier for Drug Delivery. *Soft Matter* **2011**, *7*, 6222–6230. [CrossRef]
22. Zhao, Y.; Jayachandran, M.; Xu, B. In Vivo Antioxidant and Anti-Inflammatory Effects of Soluble Dietary Fiber Konjac Glucomannan in Type-2 Diabetic Rats. *Int. J. Biol. Macromol.* **2020**, *159*, 1186–1196. [CrossRef] [PubMed]
23. Thangavel, P.; Kanniyappan, H.; Chakraborty, S.; Chaudhary, S.; Wallepure, A.; Muthuvijayan, V. Fabrication of Konjac Glucomannan-Silk Fibroin Based Biomimetic Scaffolds for Improved Vascularization and Soft Tissue Engineering Applications. *J. Appl. Polym. Sci.* **2023**, *140*, e54333. [CrossRef]
24. Wu, C.; Li, Y.; Du, Y.; Wang, L.; Tong, C.; Hu, Y.; Pang, J.; Yan, Z. Preparation and Characterization of Konjac Glucomannan-Based Bionanocomposite Film for Active Food Packaging. *Food Hydrocoll.* **2019**, *89*, 682–690. [CrossRef]
25. Zhang, R.; Wang, X.; Li, L.; Cheng, M.; Zhang, L. Optimization of Konjac Glucomannan/Carrageenan/Nano-SiO2 Coatings for Extending the Shelf-Life of Agaricus Bisporus. *Int. J. Biol. Macromol.* **2019**, *122*, 857–865. [CrossRef] [PubMed]
26. Zhang, W.; Rhim, J.-W. Recent Progress in Konjac Glucomannan-Based Active Food Packaging Films and Property Enhancement Strategies. *Food Hydrocoll.* **2022**, *128*, 107572. [CrossRef]
27. *JIS K 6251:2017*; Rubber, Vulcanized or Thermoplastic. Determination of Tensile Stress-Strain Properties. Japanese Standards Association: Tokyo, Japan, 2017.
28. *JIS K 7161-1:2014*; Plastics—Determination of Tensile Properties—Part 1: General Principles. Japanese Standards Association: Tokyo, Japan, 2014.

29. *JIS Z 0208:1976*; Testing Method for Water Vapor Transmission of Moisture-Proof Packaging Materials (Cup Method). Japanese Standards Association: Tokyo, Japan, 1976.
30. Schmidt, V.C.R.; Porto, L.M.; Laurindo, J.B.; Menegalli, F.C. Water Vapor Barrier and Mechanical Properties of Starch Films Containing Stearic Acid. *Ind. Crops Prod.* **2013**, *41*, 227–234. [CrossRef]
31. Mali, S.; Grossmann, M.V.E.; Garcıía, M.A.; Martino, M.N.; Zaritzky, N.E. Barrier, Mechanical and Optical Properties of Plasticized Yam Starch Films. *Carbohydr. Polym.* **2004**, *56*, 129–135. [CrossRef]
32. Hagiri, M.; Kanari, M.; Morota, M.; Kashima, K. Activated Carbon–Embedded Free-Standing Glucomannan Membrane for Efficient Dye Removal. *Clean. Eng. Technol.* **2026**, *31*, 101165. [CrossRef]
33. Guéout, M.A. Sur Les Dimensions Des Intervalles Poreux Des Membranes. *Comptes Rendus Hebd. Séances Académie Sci.* **1872**, *75*, 1809–1814.
34. Bjerrum, N.; Manegold, E. Ueber Kollodium-Membranen, II: Der Zusammenhang zwischen Membranstruktur und Wasserdurchlässigkeit. *Kolloid-Z.* **1927**, *43*, 5–14. [CrossRef]
35. Wilke, C.R.; Chang, P. Correlation of Diffusion Coefficients in Dilute Solutions. *AIChE J.* **1955**, *1*, 264–270. [CrossRef]
36. Ye, X.; Kennedy, J.F.; Li, B.; Xie, B.J. Condensed State Structure and Biocompatibility of the Konjac Glucomannan/Chitosan Blend Films. *Carbohydr. Polym.* **2006**, *64*, 532–538. [CrossRef]
37. Warkoyo; Purnomo, I.; Siskawardani, D.D.; Husna, A. The Effect of Konjac Glucomannan and Aloe Vera Gel Concentration on Physical and Mechanical Properties of Edible Film. *Food Res.* **2022**, *6*, 298–305. [CrossRef]
38. Xiong, R.; Zhou, J. Regenerated Cellulose Films Coated with Waterborne Polyurethane with Enhanced Mechanical Properties. *Polymers* **2025**, *17*, 890. [CrossRef]
39. Ruckenstein, E.; Li, H. The Tensile Behaviour and Toughness of Poly(Vinylidene Chloride)/Poly(Butyl Methacrylate) Composites Prepared by the Concentrated Emulsion Approach. *Polymer* **1994**, *35*, 4343–4348. [CrossRef]
40. Perera, K.Y.; Jaiswal, A.K.; Jaiswal, S. Biopolymer-Based Sustainable Food Packaging Materials: Challenges, Solutions, and Applications. *Foods* **2023**, *12*, 2422. [CrossRef] [PubMed]
41. Wei, X.; Pang, J.; Zhang, C.; Yu, C.; Chen, H.; Xie, B. Structure and Properties of Moisture-Resistant Konjac Glucomannan Films Coated with Shellac/Stearic Acid Coating. *Carbohydr. Polym.* **2015**, *118*, 119–125. [CrossRef] [PubMed]
42. Shellhammer, T.H.; Krochta, J.M. Whey Protein Emulsion Film Performance as Affected by Lipid Type and Amount. *J. Food Sci.* **1997**, *62*, 390–394. [CrossRef]
43. Aburabie, J.H.; Puspasari, T.; Peinemann, K.-V. Alginate-Based Membranes: Paving the Way for Green Organic Solvent Nanofiltration. *J. Membr. Sci.* **2020**, *596*, 117615. [CrossRef]
44. Li, C.; Wu, J.; Shi, H.; Xia, Z.; Sahoo, J.K.; Yeo, J.; Kaplan, D.L. Fiber-Based Biopolymer Processing as a Route toward Sustainability. *Adv. Mater.* **2022**, *34*, 2105196. [CrossRef]
45. Cavalcante, J.; Oldal, D.G.; Peskov, M.V.; Beke, A.K.; Hardian, R.; Schwingenschlögl, U.; Szekely, G. Biobased Interpenetrating Polymer Network Membranes for Sustainable Molecular Sieving. *ACS Nano* **2024**, *18*, 7433–7443. [CrossRef]
46. Hardian, R.; Alammar, A.; Holtzl, T.; Szekely, G. Fabrication of Sustainable Organic Solvent Nanofiltration Membranes Using Cellulose–Chitosan Biopolymer Blends. *J. Membr. Sci.* **2022**, *658*, 120743. [CrossRef]

Disclaimer/Publisher's Note: The statements, opinions and data contained in all publications are solely those of the individual author(s) and contributor(s) and not of MDPI and/or the editor(s). MDPI and/or the editor(s) disclaim responsibility for any injury to people or property resulting from any ideas, methods, instructions or products referred to in the content.